

Ultradispersive adaptive prism based on a coherently prepared atomic medium

Vladimir A. Sautenkov,^{1,2} Hebin Li,¹ Yuri V. Rostovtsev,^{3,*} and Marlan O. Scully^{1,4}

¹*Department of Physics and Institute for Quantum Studies, Texas A&M University, College Station, Texas 77843-4242, USA*

²*P. N. Lebedev Institute of Physics, Moscow 119991, Russia*

³*Department of Physics, University of North Texas, 1155 Union Circle, No. 311427, Denton, Texas 76203, USA*

⁴*College of Engineering and Applied Science, Princeton University, Princeton, NJ 08544, USA*

(Received 30 July 2009; revised manuscript received 23 February 2010; published 23 June 2010)

We have experimentally demonstrated an ultra-dispersive optical prism made from a coherently driven Rb atomic vapor. The prism possesses spectral angular dispersion that is 6 orders of magnitude higher than that of a prism made of optical glass; such angular dispersion allows one to spatially resolve light beams with different frequencies separated by a few kilohertz. The prism operates near the resonant frequency of atomic vapor and its dispersion is optically controlled by a coherent driving field.

DOI: [10.1103/PhysRevA.81.063824](https://doi.org/10.1103/PhysRevA.81.063824)

PACS number(s): 42.50.Gy

I. INTRODUCTION

A single-frequency ray of light is bent by a prism at an angle determined by the index of refraction [see Fig. 1(a)]. As shown in [1], the dispersion of the index of refraction leads to spread of deviation angles for different light frequencies.

Optical properties of matter, such as absorption, dispersion, and a variety of nonlinear characteristics, can be manipulated by electromagnetic fields [2–7]. For example, the applied coherent fields can eliminate absorption, enhance the index of refraction [8–10], induce chirality in nonchiral media [11], produce usually forbidden forward Brillouin scattering or strong coherent backward scattering in ultradispersive resonant media [12,13], slow down or speed up light pulses [14–16], provide the optical imaging beyond diffraction limit [17], and the optical analog of Stern-Gerlach experiment [18]. Optically controlled giant nonlinearities may generate nonlinear signals using single photons [19,20]. The enhanced nonlinearity can be employed for quantum information storage [21] and for manipulation of light propagating through a resonant medium, such as stationary pulses of light in an atomic medium [22].

Here we experimentally demonstrate an ultradispersive prism (we refer to it as “a prism” because it deflects light; see Fig. 1). The prism is made of a coherently driven atomic Rb vapor [4] that has a spectral angular dispersion ($d\theta/d\lambda \simeq 10^3 \text{ nm}^{-1}$) at least 6 orders of magnitude higher than that of glass prisms ($d\theta/d\lambda \simeq 10^{-4} \text{ nm}^{-1}$) or diffraction gratings ($d\theta/d\lambda \simeq 10^{-3} \text{ nm}^{-1}$).

The physics of refraction of the ultradispersive coherently driven atomic medium is based on exciting quantum coherence. The wave vector k depends on the light frequency ν as

$$k = \frac{\nu}{c}n, \quad (1)$$

where n is the index of refraction. Assuming that the driving field has an inhomogeneous profile, then the index of refraction has a spatial gradient. The light ray trajectories in

an inhomogeneous medium can be found by solving an eikonal equation [23] given by

$$(\vec{\nabla} \Psi)^2 = k^2 = \frac{\nu^2}{c^2}n^2, \quad (2)$$

where Ψ is the phase of electromagnetic wave. Then the light turning angle can be estimated as

$$\theta \simeq L\nabla n. \quad (3)$$

where $n = \sqrt{1 + 4\pi\chi_v}$, L is the length of a medium, and ∇n is the gradient of the index of refraction in the direction perpendicular to propagation. The atomic susceptibility of a coherently driven three-level medium χ_v [4] is given by

$$\text{Re}[\chi_v] = \eta\delta\omega \frac{\Omega_2^2 - \gamma_{cb}^2 - \delta\omega^2}{(\Omega_2^2 + \gamma_{cb}\gamma - \delta\omega^2)^2 + \delta\omega^2(\gamma_{cb} + \gamma)^2}, \quad (4)$$

where $\eta = 3\lambda^3 N\gamma_r/16\pi^2$, N is the density of Rb vapor, γ_r is the spontaneous emission rate, γ is the relaxation rate at optical transition, γ_{cb} is the relaxation rate at the long-lived lower frequency (spin) transition, Ω_2 is the Rabi frequency of control field, ν is the frequency of the probe field, $\delta\omega = \nu - \omega_{ab}$ is the detuning of the probe field from atomic transition $\omega_{ab} = 2\pi c/\lambda$; and λ is the wavelength of the resonant transition. Then, for realistic parameters, such as $\delta\omega \simeq 1 \times 10^3 \text{ s}^{-1}$, $\gamma_{cb} = 1 \times 10^3 \text{ s}^{-1}$, $N \simeq 10^{13} \text{ cm}^{-3}$, and $L = 10 \text{ cm}$, the estimate yields $\theta \simeq 0.1$, which shows a lot of potential for implementation of the predicted effect. Note here that the spatial dependence of gradient of the driving field is important and, also, that the effect can be increased even more by using an enhanced index of refraction without absorption [8–10].

II. EXPERIMENTAL SETUP AND RESULTS

A schematic of an experimental setup is shown in Fig. 2. We have used a highly coherent extended-cavity diode laser (ECDL) [20] that is tuned to the center of the Doppler broadened hyperfine component of the D1 line of ^{87}Rb [the transition $5S_{1/2}(F=2) - 5P_{1/2}(F'=1)$]. A part of the output laser is used to control the laser frequency by observing the Doppler-free saturation resonance in the rubidium reference

*rost@unt.edu

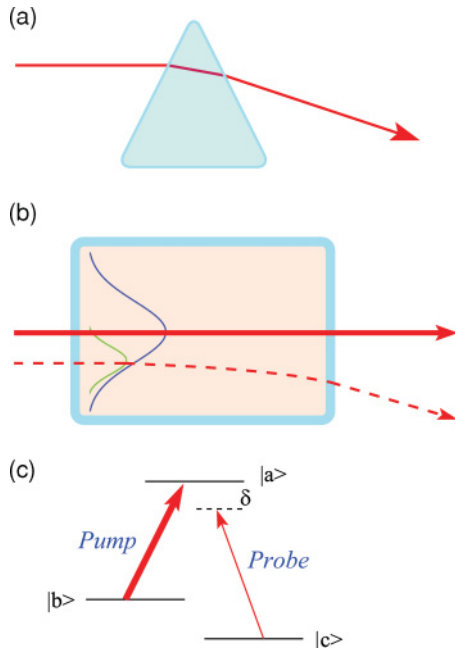


FIG. 1. (Color online) (a) Refraction of light by the prism. (b) Configuration of the probe and control laser beams inside the cell of Rb vapor. One can see that our setup can be viewed as an ultradispersive prism. (c) Simplified scheme of the energy levels of Rb atoms.

cell, which serves as the frequency reference. Another part of the laser output is used to study the ultradispersive optical prism. The beam is split into two beams, and the $\lambda/2$ wave plate rotates the linear polarization of one beam by 90° . After passing through a polarizing beam splitter (PBS) and the $\lambda/4$ wave plate, the laser beams are sent to the glass cell with rubidium atomic vapor. The configuration of the laser beams in the cell is shown in Fig. 1(b). The orthogonally polarized beams, control ($P_c = 0.5$ mW) and probe ($P_p = 0.2$ mW), create coherence between the ground-state Zeeman sublevels as shown in Fig. 1(c). Two-photon detuning is accomplished by applying the longitudinal magnetic field B . The magnitude of Zeeman splitting is given by $0.7 B$ MHz/G. The heated rubidium cell ($l = 7.5$ cm, $N = 3 \times 10^{11}$ cm $^{-3}$) is

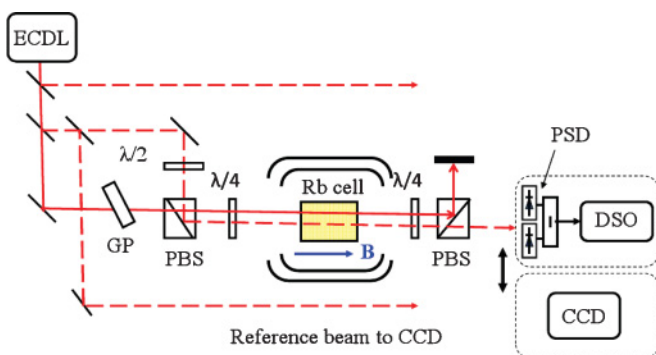


FIG. 2. (Color online) Experimental setup: ECDL, external cavity diode laser; PBS, polarizing beam splitter; GP, parallel glass plate; $\lambda/2$ and $\lambda/4$, retardation wave plates; PSD, position-sensitive detector; DSO, the digital storage oscilloscope; CCD, linear CCD camera.

installed inside of a two-layer magnetic shield, and two-photon detuning is varied by changing the magnitude of the longitudinal magnetic field. The transmitted optical beams with the orthogonal polarizations are separated using a second $\lambda/4$ wave plate and another PBS. Then the probe beam is sent to the data acquisition part of the setup.

We employ two independent techniques to measure the probe beam position and the angle of deviation. Measurements by both techniques are consistent with each other. The first technique is based on using a charge-coupled device (CCD) camera and a removable mirror in front of the cell to measure the positions of the control and probe beams. The CCD camera is used to record an optical field distribution for selected two-photon detuning. In the second method, we use a position-sensitive detector (PSD) [21] to accurately measure the beam direction versus the two-photon detuning. The distance from the center of the cell to PSD is 1 m, and that to the CCD camera is 2.3 m. The influence of air currents on the beams around the heated cell is negligible due to the small variation of temperature inside the magnetic shield ($L = 0.4$ m). In addition, the optical paths are protected by covers.

To study the frequency dependence of the probe beam deflection, we record a signal from the PSD. The output voltage from the PSD is proportional to the transverse shift of the beam. The relation between the shift of the probe beam and the signal from the PSD is calibrated by using a translation stage. Before the cell, the control and probe beams are parallel to each other. The control beam can be adjusted to the left or to the right side of the probe beam profile by tilting a parallel glass plate. The profiles of the beams are shown in Fig. 3(a) for the case when the probe beam is shifted to the right side of the control beam. The profiles have been recorded by the CCD camera. Dependence of the angle of the probe beam refraction on two-photon detuning for the probe beam is presented in Fig. 4(a) as curve 1. The curve is dispersion-like and it has a maximum and minimum at 0.5 and -0.2 mrad, respectively. In addition, we have recorded the transmission of the probe beam by using a removable mirror and a usual photo detector. The EIT resonance is presented in Fig. 4(a) as curve 2. Then we shift the probe beam to the left side of the control beam profile. Frequency dependence of the angle and EIT resonance is presented in Fig. 4(b). The dispersion-like curve 1 has a maximum and minimum at 0.05 and -0.45 mrad. The widths (FWHMs) of EIT resonances are 0.5 MHz for the both cases. The different offset for dispersion-like curves in Figs. 4(a) and 4(b) can be attributed to single-photon saturation of rubidium atoms. Near zero detuning, the dependences are practically linear. They can be characterized by slopes $d\theta/d\nu$, which can be estimated using the preceding parameters to be of the order of 1 mrad/MHz. By using the obtained values of the slopes at zero detuning, we can estimate $d\theta/d\lambda$ as 5×10^2 rad/nm.

The profiles of the probe beam after the rubidium cell are recorded by the CCD camera. For the case when the probe beam is on the right side of the pump beam the profiles of the probe beams before the cell for two different two-photon detunings are presented in Fig. 3(b). Curve 2' in Fig. 3(b) corresponds to the maximum angle deviation in Fig. 4(a) ($\theta = 0.5$ mrad) and curve 2 in Fig. 3(b) corresponds to the minimum

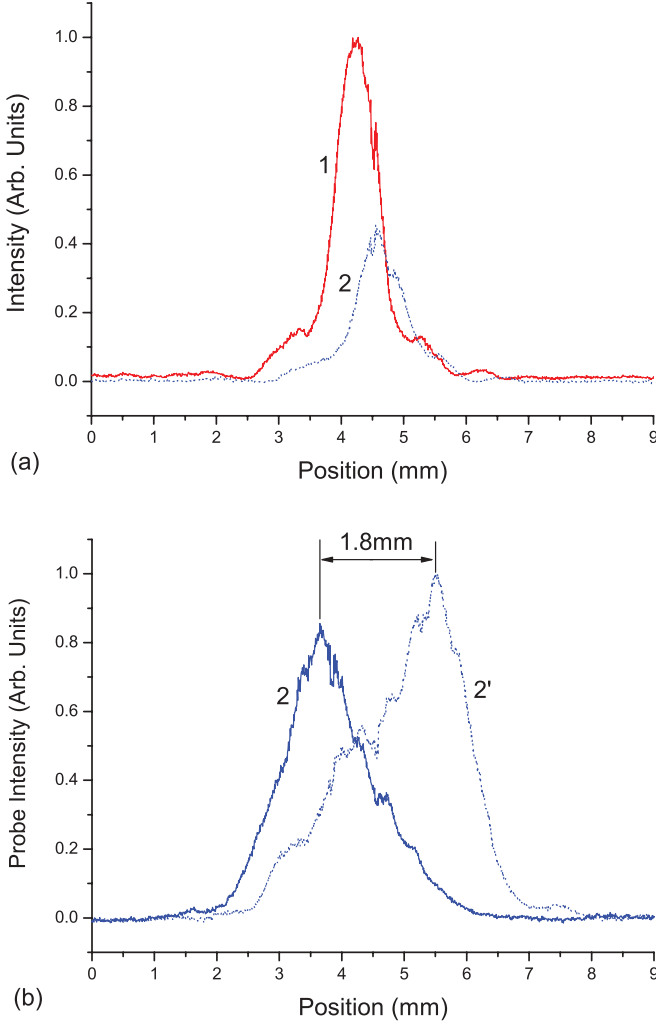


FIG. 3. (Color online) (a) Spatial distributions of the control (1) and probe (2) fields at the input of the atomic cell (we have no magnification of the optical beams). The probe is shifted to the right with respect to the control field. (b) Spatial distributions of the probe fields (2) and (2') at the distance of 2.3 m after passing the atomic cell for different detunings corresponding to the maximal angles of deviation.

angle deviation in Fig. 4(a) ($\theta = -0.2$ mrad). The width of the probe beam is increased at a 2.3-m distance from the cell due to diffraction (the diffraction opening for a Gaussian beam profile is given by $2\lambda/\pi r$, where r is the radius of the laser beam). For the data shown in Fig. 3(b), the displacement due to the prism effect is larger than the spread of the probe beam due to diffraction. The interval of 1.8 mm between the beam profiles is in a good agreement with the angle deviation in Fig. 4(a). The resolution and deflection angle can be increased by using the rubidium cell with buffer gas, where the width of EIT resonance can be reduced to 1 kHz. The results of the simulations are discussed in Sec. III.

III. THEORY

The trajectory of the light rays propagating in an inhomogeneous medium can be found by using the eikonal

approximation [23]. Starting with the Maxwell equation, which describes propagation of electromagnetic waves as

$$\Delta E - \frac{1}{c^2} \frac{\partial^2 E}{\partial t^2} = \frac{4\pi}{c^2} \frac{\partial^2 P}{\partial t^2}, \quad (5)$$

and presenting the field and the polarization as

$$E = \sum_{\nu} E_{\nu} e^{-i\nu t + ik\psi}, \quad P = \sum_{\nu} P_{\nu} e^{-i\nu t + ik\psi}, \quad (6)$$

where the ψ is the eikonal, the polarization of the medium is related to the field intensity as $P_{\nu} = \chi_{\nu} E_{\nu}$, where the susceptibility χ_{ν} is $\chi_{\nu} = \chi'_{\nu} + i\chi''_{\nu}$. Neglecting the second-order derivative over coordinates for amplitude E_{ν} , we obtain the eikonal equation given by

$$(\nabla\psi)^2 = 1 + 4\pi\chi'_{\nu}. \quad (7)$$

The trajectory of the light rays propagating in an inhomogeneous medium can be found by solving a geometrical optics differential equation [23] that is given in vector form by

$$\frac{d}{ds} \left(n \frac{d\vec{R}}{ds} \right) = \nabla n, \quad (8)$$

where \vec{R} is the the point of the ray, and n is the index of refraction defined as $n^2 \equiv 1 + 4\pi\chi'_{\nu}$. $\vec{R}(x, z) = X(z)\hat{x} + z\hat{z}$, \hat{x} and \hat{z} are the unit vectors along the axis. Then, for the x and z components,

$$\frac{d}{ds} \left(n \frac{dX}{ds} \right) = \frac{\partial n}{\partial x}, \quad \frac{d}{ds} \left(n \frac{dz}{ds} \right) = \frac{\partial n}{\partial z}. \quad (9)$$

The equation describing the amplitude of the electromagnetic field can be obtained similarly to how we obtain Eq. (7), and it is given by

$$2ik\nabla\psi\nabla E_{\nu} + ik\nabla^2\psi E_{\nu} = -\frac{4\pi\nu^2}{c^2} \chi''_{\nu} E_{\nu}. \quad (10)$$

The solution of the above equation has the following form:

$$E_{\nu} = \frac{E_{0\nu}}{\sqrt{n}} \exp\left(-\int_{s_1}^{s_2} \frac{2\pi\nu\chi''_{\nu}}{nc} ds\right). \quad (11)$$

The light turning angle θ can be estimated by

$$\theta = \frac{\omega - \omega_{ab}}{kV_g} \frac{\Delta V_g}{V_g} \frac{L}{D} = \frac{\omega - \omega_{ab}}{\gamma_{cb} k D} \frac{\Delta V_g}{V_g} \frac{\gamma_{cb} L}{V_g}, \quad (12)$$

where we use $\frac{\partial V_g}{\partial z} \simeq \frac{\Delta V_g}{D}$, D is the diameter of the beam, the length of the sample is determined by residual absorption κ , indeed, $\kappa L = \frac{\gamma_{cb} + (\Omega^2/\gamma)}{V_g} L \sim 1$, and for realistic parameters $\omega - \omega_{ab} \simeq 10^8$ s⁻¹, $\gamma_{cb} = 10^3$ s⁻¹, and $kD \simeq 10^5 \times 0.1 \simeq 10^4$, V_g can be of the order of 100 m/s, the estimation gives us $\theta \simeq 0.1$, which shows a lot of potential for all-optical light steering.

We perform simulation using the density matrix approach and the parameters of our experiment. The interaction Hamiltonian of the system can be written as

$$V_I = -\hbar[\Omega_1 e^{-i\omega_{ab}t} |a\rangle\langle b| + \Omega_2 e^{-i\omega_{act}} |a\rangle\langle c| + \text{H.c.}], \quad (13)$$

where $\Omega_{1,2} = \wp_{1,2} \mathcal{E}_{1,2} / \hbar$ is the Rabi frequency of the probe (drive) field, and ω_{ab} , ω_{ac} , ω_{cb} are the frequency differences

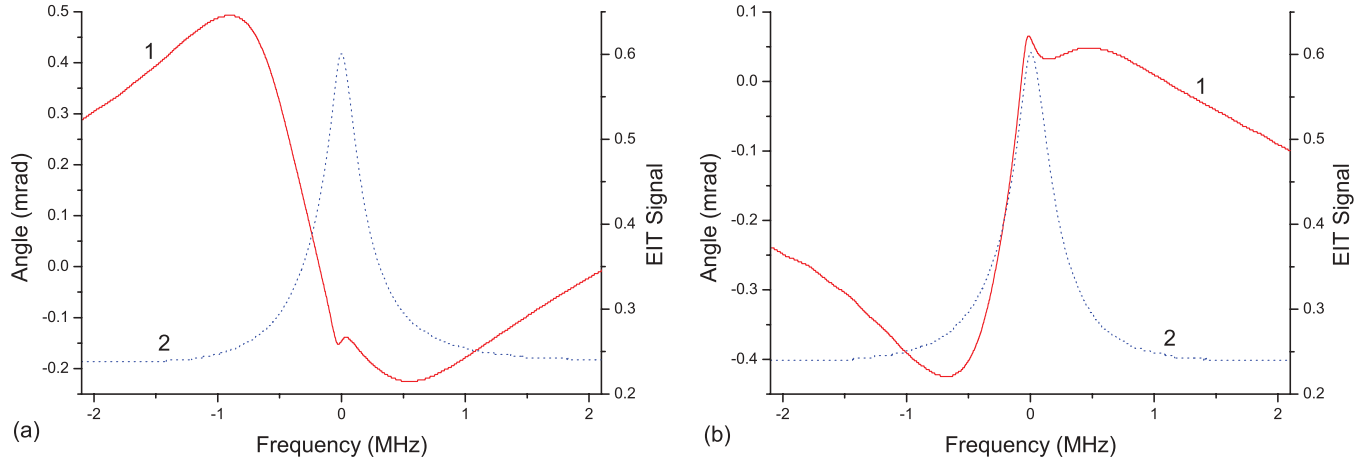


FIG. 4. (Color online) Curve 1: Dependence of the deflection angle of the probe beam on detuning for the probe beam initially shifted to the right (a) and to the left (b) with respect to the control beam. Curve 2: Dependence of the probe field transmission versus detuning.

between the corresponding atomic energy levels (see Fig. 1). The time-dependent density matrix equations are given by

$$\frac{\partial \rho}{\partial t} = -\frac{i}{\hbar}[V_I, \rho] - \frac{1}{2}(\Gamma \rho + \rho \Gamma), \quad (14)$$

where Γ is the relaxation matrix. A self-consistent system also includes the field propagation equations

$$\frac{\partial \Omega_1}{\partial z} = -iG_1 \rho_{ab}, \quad \frac{\partial \Omega_2}{\partial z} = -iG_2 \rho_{ac}, \quad (15)$$

where $G_j = 2\pi N g_j^2 v_j / c$ are the coupling constants ($j = 1, 2$), and N is the particle density of the medium. The equations of motion for the density matrix elements of the polarization ρ_{ab} and the coherence ρ_{cb} are given by

$$\dot{\rho}_{ab} = -\Gamma_{ab} \rho_{ab} + i\Omega_1(\rho_{aa} - \rho_{bb}) - i\rho_{cb}\Omega_2^*, \quad (16)$$

$$\dot{\rho}_{cb} = -\Gamma_{cb} \rho_{cb} + i\rho_{ca}\Omega_1 - i\rho_{ab}\Omega_2, \quad (17)$$

where $\Gamma_{ab} = \gamma_{ab} + i(\omega_{ab} - \nu_1)$, $\Gamma_{ca} = \gamma_{ca} - i(\omega_{ac} - \nu_2)$, $\Gamma_{cb} = \gamma_{cb} + i(\omega_{cb} - \nu_1 + \nu_2)$, ω_{cb} is the frequency of the c - b transition, and $\gamma_{\alpha\beta}$ are the relaxation rates of coherence at the corresponding transitions.

Assuming that the drive field is much stronger than the probe field ($|\Omega_1|^2 \ll |\Omega_2|^2$), then $\rho_{bb} \simeq 1$, and the susceptibility is given by

$$\chi_{v_1} = \frac{-i\eta\Gamma_{cb}}{\Gamma_{ab}\Gamma_{cb} + |\Omega_2|^2}. \quad (18)$$

The index of refraction is $n \simeq 1 + 2\pi \text{Re}[\chi_{v_1}]$, and the angle of refraction can be found by solving

$$\frac{\partial \tan \theta}{\partial z} = 2\pi \frac{\partial \chi'_{v_1}}{\partial x} = \text{Re} \left[\frac{2\pi i \eta \Gamma_{cb}}{(\Gamma_{cb} \Gamma_{ab} + |\Omega_2|^2)^2} \right] \frac{\partial |\Omega_2|^2}{\partial x}. \quad (19)$$

For our case the refraction angle is small, so $\tan \theta \simeq \theta$, and is given by

$$\theta = 2\pi \int_0^L dz \frac{\partial \chi'_{v_1}}{\partial x}, \quad (20)$$

where L is the length of the cell.

The numerical results are shown in Fig. 5. We use the following parameters for the simulations: the atomic density

is $N = 3 \times 10^{11} \text{ cm}^{-3}$, the Doppler width is $\Delta_D = 500 \text{ MHz}$, the homogeneous broadening of optical transitions is purely due to the radiative broadening determined by spontaneous relaxation and is given by $\gamma_r = 6 \text{ MHz}$, the spin transition relaxation is $\gamma_{cb} = 0.01\gamma_r \text{ kHz}$, determined by the time-of-flight broadening (direct measurement of spin relaxation for our setup is given in [30]), and the Rabi frequency of the driving field $\Omega_2 = 4\gamma_r$. The simulations reproduce perfectly the experimental results as well as the features that can be seen in the experimental plots in Fig. 3 at zero detuning.

The observed feature is paradoxical. Indeed, the dispersion of the probe beam at the center of the optical line is 0 [see Eq. (18)], hence the derivative should be 0 too. On the contrary, we have observed the refraction of the probe beam at the zero frequency. The explanation is the following. The feature appears to be due to spatial inhomogeneity of the driving field, which results in a reshaping of the probe beam such that the position of the maximum spatial distribution of the probe beam experiences a shift during propagation through the medium with inhomogeneous distribution of the drive field. The shift in the maximum of the probe beam distribution depends on

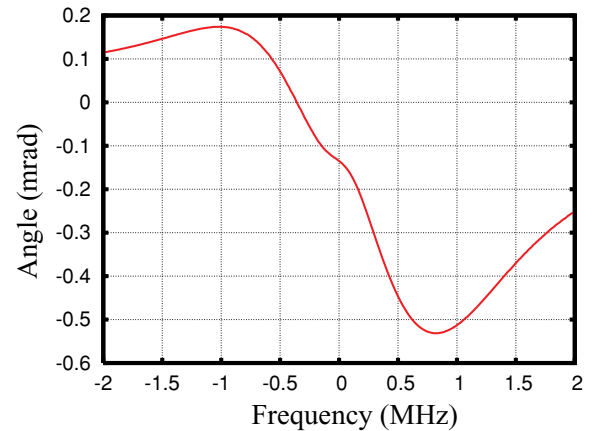


FIG. 5. (Color online) Calculated dependence of the deflection angle of the probe beam on detuning for the probe beam vs. two-photon detuning.

two-photon detuning and explains “refraction” of the probe beam at zero detuning. We find the shift of the beam by solving Eq. (15) (the shift is of the order of the spatial width of the probe beam at two-photon resonance). Taking this shift into account reproduces satisfactorily the feature experimentally observed.

Also, here we should note that in order for the setup to be considered as a prism with a high-frequency dispersion, the different frequencies should be spatially resolved, which establishes a condition on the diameter of the optical beams. The spatial resolution should match the spectral resolution. Without such matching the device would just deflect the optical beam at the same angle, without separation for different frequencies. Thus, the condition for being able to observe the frequency separation of the probe beam is $\delta\phi \simeq \frac{d\phi}{d\lambda}\delta\lambda > \frac{\lambda}{D}$ (D is the diameter of the probe beam); the angular separation due to frequency dispersion should be bigger than the diffraction of the beam. The optical beams should be wider than $D > \frac{v_p}{\gamma_{cb}(d\phi/d\lambda)} = 2$ mm, which is experimentally doable.

IV. CONCLUSION

In conclusion, we have experimentally demonstrated an EIT prism yielding large angular dispersion. The obtained results show the dependence of the angle of deviation on the detuning that is introduced by a magnetic field. It follows from Eq. (3) that the angle of deviation is related to the dispersion of the medium and the space gradient. Alternating the sign of the spacial gradient by shifting the probe beam, we can see the change in the dependence of the angle of deviation on the two-photon detuning.

The scheme holds promise for many applications. Such ultrahigh-frequency dispersion could be used for a compact

high spectral resolution spectrometer, similar to compact atomic clocks and magnetometers [29]. The prism has a huge angular dispersion ($d\theta/d\lambda = 10^3 \text{ nm}^{-1}$), which can spatially resolve spectral widths of a few kilohertz, with a corresponding spectral resolution $R = \lambda/\delta\lambda \simeq 10^{12}$ (One can see that our approach hold promise; indeed recently, for example, the 1-mm-length spectrometer has shown a resolution of 400 [28]). We have observed the angle of deviation to be an order of magnitude larger than the one previously observed in an inhomogeneous magnetic field [18]. We emphasize that the angle can be increased even further by using the enhanced index of refraction without absorption [8–10].

The ability to control the direction of light propagation by another light beam in transparent medium can be applied to optical imaging and to all-optical light steering [27]. Also, this prism can be used for all-optical controlled delay lines for radar systems. This technique can be easily extended to short pulses by using the approach developed in [26].

In contrast, together with its application to relatively intense classical fields, the ultradispersive prism can be applied to weak fields, such as a single-photon source, and control of the flow of photons at the level of a single quantum [19,20].

ACKNOWLEDGMENTS

We thank Hui Chen and M. Suhail Zubairy for useful discussions and gratefully acknowledge support from the CRDF, Defense Advanced Research Projects, NSF Grant No. EEC-0540832 (MIRTHE ERC), the Office of Naval Research, and the Robert A. Welch Foundation (Award No. A-1261).

-
- [1] Isaac Newton, *Opticks: Or a Treatise of the Reflections, Refractions, Inflections and Colours of Light*, 4th ed. (London, 1730); reprinted (1952), by Dover, New York.
 - [2] E. Arimondo, in *Progress in Optics*, edited by E. Wolf (Elsevier, Amsterdam, 1996), Vol. XXXV, pp. 257–354.
 - [3] S. E. Harris, *Phys. Today* **50**, 36 (1997).
 - [4] M. O. Scully and M. S. Zubairy, *Quantum Optics* (Cambridge University Press, Cambridge, UK, 1997).
 - [5] V. A. Sautenkov, Y. V. Rostovtsev, C. Y. Ye, G. R. Welch, O. Kocharovskaya, and M. O. Scully, *Phys. Rev. A* **71**, 063804 (2005).
 - [6] E. E. Mikhailov, V. A. Sautenkov, Y. V. Rostovtsev, A. Zhang, M. S. Zubairy, M. O. Scully, and G. R. Welch, *Phys. Rev. A* **74**, 013807 (2006).
 - [7] H. Li, V. A. Sautenkov, Y. V. Rostovtsev, G. R. Welch, P. R. Hemmer, and M. O. Scully, *Phys. Rev. A* **80**, 023820 (2009).
 - [8] M. O. Scully, *Phys. Rev. Lett.* **67**, 1855 (1991).
 - [9] A. S. Zibrov, M. D. Lukin, L. Hollberg, D. E. Nikonov, M. O. Scully, H. G. Robinson, and V. L. Velichansky, *Phys. Rev. Lett.* **76**, 3935 (1996).
 - [10] U. Rathe, M. Fleischhauer, S.-Y. Zhu, T. W. Hansch, and M. O. Scully, *Phys. Rev. A* **47**, 4994 (1993).
 - [11] V. A. Sautenkov, Y. V. Rostovtsev, H. Chen, P. Hsu, G. S. Agarwal, and M. O. Scully, *Phys. Rev. Lett.* **94**, 233601 (2005).
 - [12] A. B. Matsko, Y. V. Rostovtsev, M. Fleischhauer, and M. O. Scully, *Phys. Rev. Lett.* **86**, 2006 (2001).
 - [13] Y. V. Rostovtsev, Z. E. Sariyanni, and M. O. Scully, *Phys. Rev. Lett.* **97**, 113001 (2006).
 - [14] A. B. Matsko, O. Kocharovskaya, Y. Rostovtsev, G. R. Welch, A. S. Zibrov, and M. O. Scully, *Adv. At. Mol. Opt. Phys.* **46**, 191 (2001).
 - [15] R. W. Boyd, *Prog. Opt.* **43**, 497 (2002).
 - [16] G. M. Gehring, A. Schweinsberg, C. Barsi, N. Kostinski, and R. W. Boyd, *Science* **312**, 895 (2006).
 - [17] H. Li, V. A. Sautenkov, M. M. Kash, A. V. Sokolov, G. R. Welch, Y. V. Rostovtsev, M. S. Zubairy, and M. O. Scully, *Phys. Rev. A* **78**, 013803 (2008).
 - [18] L. Karpa and M. Weitz, *Nature Phys.* **2**, 332 (2006).
 - [19] S. E. Harris and Y. Yamamoto, *Phys. Rev. Lett.* **81**, 3611 (1998).
 - [20] V. Balic, D. A. Braje, P. Kolchin, G. Y. Yin, and S. E. Harris, *Phys. Rev. Lett.* **94**, 183601 (2005).
 - [21] C. H. van der Wal, M. D. Eisaman, A. Andre, R. L. Walsworth, D. F. Phillips, A. S. Zibrov, and M. D. Lukin, *Science* **301**, 196 (2003).
 - [22] M. Bajcsy, A. S. Zibrov, and M. D. Lukin, *Nature (London)* **426**, 638 (2003).
 - [23] M. Born and E. Wolf, *Principles of Optics: Electromagnetic Theory of Propagation, Interference and Diffraction*

- of Light* (Cambridge University Press, Cambridge, UK, 1997).
- [24] V. A. Sautenkov, Yu. V. Rostovtsev, and M. O. Scully, *Phys. Rev. A* **72**, 065801 (2005).
- [25] R. Schlessler and A. Weis, *Opt. Lett.* **17**, 1015 (1992).
- [26] Q. Sun, Y. V. Rostovtsev, J. P. Dowling, M. O. Scully, and M. S. Zubairy, *Phys. Rev. A* **72**, 031802(R) (2005).
- [27] Q. Sun, Y. V. Rostovtsev, and M. S. Zubairy, *Phys. Rev. A* **74**, 033819 (2006).
- [28] E. Le Coarer, S. Blaize, P. Benech, I. Stefanon, A. Morand, G. Lerondel, G. Leblond, P. Kern, J. M. Fedeli, and P. Royer, *Nature Photon.* **1**, 473 (2007).
- [29] S. Knappe, P. D. D. Schwindt, V. Gerginov, V. Shah, L. Liew, J. Moreland, H. G. Robinson, L. Hollberg, and J. Kitching, *J. Opt. A* **8**, S318 (2006).
- [30] V. A. Sautenkov, H. Li, Y. V. Rostovtsev, G. R. Welch, J. P. Davis, F. A. Narducci, and M. O. Scully, *J. Mod. Opt.* **56**, 975 (2009).